Computational and Structural Biotechnology Journal 20 (2022) 386–398

COMPUTATIONAL AND STRUCTURAL BIOTECHNOLOGY JOURNAL

journal homepage: www.elsevier.com/locate/csbj

Advanced biokinetic and hydrodynamic modelling to support and optimize the design of full-scale high rate algal ponds

Antonio Ortiz [a], Rubén Díez-Montero [a], Joan García [a], Nadeem Khalil [b], Enrica Uggetti [a,*]

[a] GEMMA-Group of Environmental Engineering and Microbiology, Department of Civil and Environmental Engineering, Universitat Politècnica de Catalunya-BarcelonaTech. c/ Jordi Girona 1-3, Building D1, E-08034 Barcelona, Spain
[b] Department of Civil Engineering, Z H College of Engineering & Technology, Aligarh Muslim University, Aligarh 202001 UP India

ARTICLE INFO

Article history:
Received 12 August 2021
Received in revised form 26 December 2021
Accepted 27 December 2021
Available online 31 December 2021

Keywords:
HRAP design
Wastewater
Full-scale
Computational Fluid Dynamics
Microalgae-bacteria biokinetic modelling

ABSTRACT

High rate algal ponds (HRAP) are known for their suitability to treat wastewater and to produce microalgal biomass, which can be converted into bioproducts. However, full-scale application of HRAP is still limited to few cases, and design procedures are not consolidated or standardized. In this study, a demonstrative-scale HRAP system for secondary wastewater treatment to be implemented in India (treatment capacity of 50 $m^3 \cdot d^{-1}$) has been designed combining conventional dimensioning techniques and advanced modelling tools. The objective of the study was to assist, verify and optimize the conventional dimensioning of the secondary HRAP by means of simulations predicting the behaviour of the system in the specific local conditions under different configurations and operational strategies. Biokinetic modelling and hydrodynamic analysis using Computational Fluid Dynamics (CFD) were carried out. The simulations performed with the biokinetic model showed that the optimal hydraulic retention time to enhance nutrient removal and biomass production is 4 days. For the hydrodynamic modelling, a 3D model of the HRAP was built to simulate the hydrodynamic behaviour of 36 different designs. Simulations allowed quantifying the presence of low velocity zones as well as the land use efficiency of the different designs in terms of the useful area vs. the total occupied area. Two baffles and tear-shapes with a diameter equal to ¼ of the channel width was the most efficient configuration. Moreover, a technical–economic assessment of the system was carried out, resulting in an investment cost of 483 € per population equivalent and an operational cost of 0.19 € per m^3 of treated wastewater.

1. Introduction

Microalgae-based wastewater treatment systems are currently being investigated with renewed interest. This is due to their high capability to 1) remove nutrients, organic matter and other pollutants such as heavy metals [1], and 2) produce microalgae biomass suitable to generate bioproducts such as bioplastics [2], pigments [3,4], and biogas [5,6]. Open systems, such as high rate algal ponds (HRAPs), are the most commonly used, due to their versatility, easy operation and low operation and maintenance costs [7].

HRAPs are shallow raceway reactors in which the mixed liquor, composed by wastewater and a consortium of microalgae and bacteria, flows in a channel around a central wall, driven by a paddlewheel. In such systems, microalgae biomass grows using wastewater as culture media, fixating CO_2 from the atmosphere and assimilating the nutrients (mostly nitrogen and phosphorus) present in the influent wastewater. Through photosynthesis, microalgae generate the oxygen needed by heterotrophic and autotrophic bacteria to aerobically degrade the organic matter and ammonium present in the influent wastewater [8]. Therefore, the energy requirement is low compared to that of conventional wastewater treatment systems, such as activated sludge, since microalgae-based systems do not require external aeration due to photosynthesis [7]. Even if the efficiency of microalgae-based systems has been proved in several studies at pilot scale, this technology has not been clearly expanded to an industrial scale yet. This is mainly due to their lower efficiency when compared to conventional processes and their dependence on climatic conditions. In addition, in order to outcompete with conventional treatment systems, the hydraulic retention time (HRT) has to be reduced at least below 7 days, and the power consumption below 0.5 $kWh \cdot m^{-3}$, which is the average of conventional wastewater treatment by activated sludge [9].

* Corresponding author.
E-mail address: enrica.uggetti@upc.edu (E. Uggetti).

https://doi.org/10.1016/j.csbj.2021.12.034

Apart from the climatic conditions (e.g. solar radiation and temperature) [10,11], the successful performance and efficiency of HRAPs drastically depends on the proper biological and hydrodynamic design of the ponds [12,13]. However, in contrast with conventional activated sludge reactors, the design procedure of HRAPs is not consolidated. The dimensioning of the HRAPs is usually based on general parameters such as the HRT and organic loading rate (OLR). However, complex biological, chemical and physical processes, influenced by several environmental factors, take place in HRAPs, including interactions between microalgae and bacteria. Therefore, the eventual performance of the HRAPs can differ significantly from the expected results. Regarding the hydrodynamics, it is usually neglected in conventional dimensioning of the HRAPs, supposing ideal complete mixing flow in reactors. However, the actual hydrodynamic behaviour differs from ideal flow conditions [14], affecting the performance, treatment efficiency and energy consumption in the HRAPs. Several studies have shown that the optimization of the hydrodynamic behaviour improves the efficiency of the biological process in bioreactors for wastewater treatment [15,16,17,18].

Numerical techniques, boosted by the continuous advances in computation capacity, are being increasingly applied in the wastewater treatment field. Mathematical modelling can be used as a tool to assist and verify the design and optimization of wastewater treatment systems, particularly in microalgae culture systems at industrial scale [19]. On the one hand, the biological activity of microalgae and bacteria can be simulated through biokinetic modelling, including complex processes and interactions between microalgae and bacteria to predict the treatment efficiency and biomass production [20]. On the other hand, a detailed evaluation of the hydrodynamic conditions of the HRAP can be performed by means of Computational Fluid Dynamics (CFD). CFD simulations allow to analyse the velocity fields, flow patterns and mixing performance, and to identify and minimize the extent of dead zones in the HRAP, where the biomass can settle, reducing the light exposure of the biomass and hampering the proper biomass harvesting. Several recent studies have been found in the literature dealing with the evaluation of the hydrodynamic conditions of different designs of HRAPs by CFD [13,14,21]. Those studies analysed how to improve the hydrodynamic behaviour by increasing the width of the central separation wall of the two channels of the HRAP, the implementation of tear-shapes at the ends of the separation wall, and the implementation of deflector baffles at the reversals [14,21]. However, the optimization of the hydrodynamic behaviour by means of the combination of those three components has not been deeply analysed.

The objective of this study was to design a full-scale HRAP for the secondary treatment of 50 m^3 per day of urban wastewater in Aligarh (India). The HRAP is proposed as the core of a treatment train consisting in pre-treatment (screening, and grit and grease removal), primary treatment (by gravity settling) and secondary treatment and nutrient removal in the HRAP. A set of two HRAPs working in parallel was proposed, with carousel-shape and paddlewheel driven water flow. Advanced biokinetic modelling was used to simulate the biological performance of the wastewater treatment process and to predict the production of biomass. CFD modelling was used to evaluate the hydrodynamic behaviour of 36 designs with different combinations of width of the central wall, tear-shapes at the ends of the central wall and number of semicircular deflector baffles, in order to optimize the design of the HRAPs. In addition, a technical–economic assessment has been performed in order to estimate the implementation and operation costs of this technology at this scale.

2. Materials and methods

2.1. Input data and treatment objectives

This study was performed within the framework of the H2020 project PAVITR (http://www.pavitr.net; GA 821410), which objective is the validation of sustainable natural and advanced technologies for water and wastewater treatment, monitoring and safe water reuse in India. Among other activities, two HRAPs operating in parallel were designed and are being implemented to treat urban wastewater after primary settling in a wastewater treatment plant located in the Campus of the Aligarh Muslim University (Aligarh, India).

For HRAPs design, average values of influent wastewater characteristic (Table 1) were obtained from previous studies carried out in the same location [22,23]. The organic load of the influent wastewater was estimated as 212 population equivalent (PE), considering a specific daily load of 40 gBOD_5 per person per day, which is considered the specific load in developing countries [24,25]. The parameters to define the working conditions in the HRAPs (water depth, total surface area and OLR) were stablished in order to produce an effluent able to meet the requirements for discharges from urban wastewater treatment plants to sensitive areas, which are subject to eutrophication set by the European Directive 91/271/EEC [27]. These requirements, including organic matter, suspended solids and nutrients (nitrogen and phosphorus) are also presented in Table 1.

The solar irradiation, photosynthetically active radiation (PAR), air temperature and precipitations in the location of the plant are presented in Table 2. These data have been obtained from [26] and from the India Meteorological Department.

The weather conditions show a solar radiation varying from 3.49 to 6.36 $kWh \cdot m^{-2} \cdot day^{-1}$ along the year. Also, the PAR was calculated from the total solar irradiation (as described in section 2.3.1) to be used in the biokinetic model and simulations. The maximum daily PAR values at midday for each month ranged between 921 and 1302 $\mu E \cdot m^{-2} \cdot s^{-1}$ along the year. Strong seasonal rain events take place in summer months due to the monsoon. The warm season occurs from March to October, with maximum temperatures over 30 °C and minimum temperatures over 10 °C along these months. Lower temperatures can be observed in the cold season, from November to February, but the minimum temperature does not fall under 7 °C (minimum of 7.1 °C achieved in January).

The treatment objective of the plant was to achieve the strictest European requirements for wastewater treatment to be discharged in areas sensitive to eutrophication [27].

Table 1
Aligarh wastewater characteristics (influent to the HRAP) and effluent requirements (according to the European Directive 91/271/EEC).

Parameter	Influent wastewater to the HRAP	Effluent requirement
Biochemical Oxygen Demand (BOD_5), $mg \cdot L^{-1}$	170	25
Chemical Oxygen Demand (COD), $mg \cdot L^{-1}$	339	125
Total Suspended Solids (TSS), $mg \cdot L^{-1}$	306	60*
Volatile Suspended Solids (VSS), $mg \cdot L^{-1}$	250	–
$N\text{-}NH_4^+$, $mg \cdot L^{-1}$	32	15 (Total N)**
$P\text{-}PO_4^{3-}$, $mg \cdot L^{-1}$	4	2 (Total P)**

* for urban agglomerations between 2,000 and 10,000 population equivalent.
** for urban agglomerations with<100,000 population equivalent.

Table 2
Weather conditions and solar radiation in Aligarh (India) (monthly averages). *Maximum daily photosynthetically active radiation (PAR) at midday for each month.

	Jan	Feb	Mar	Apr	May	Jun	Jul	Aug	Sep	Oct	Nov	Dec
Maximum temperature, °C	19.8	23.5	30.3	37.0	40.1	39.2	35.3	33.4	33.6	32.8	27.9	22.3
Minimum temperature, °C	7.1	9.5	14.3	19.9	24.2	26.3	26.0	25.2	23.5	18.4	12.6	8.3
Rainfall, mm	13.4	15.4	9.1	9.8	29.0	65.8	207.4	234.5	112.2	19.7	4.3	7.2
Rainy days	1.3	1.4	1.0	0.9	2.6	3.9	9.0	10.4	5.9	0.9	0.5	0.7
Solar irradiation, $kWh \cdot m^{-2} \cdot day^{-1}$	3.67	4.69	5.59	6.08	6.36	6.01	4.97	4.54	4.75	4.73	4.03	3.49
PAR, $\mu E \cdot m^{-2} \cdot s^{-1*}$	921	1177	1294	1302	1291	1190	994	948	1063	1152	1069	968

2.2. Sizing of the HRAPs

The sizing of the HRAPs consisted in the determination of the HRAPs volume and the power of the paddlewheels to allow for a proper operation and to achieve the desired treatment efficiency given the input data and conditions. To this aim, both biological and hydraulic sizing have been performed. Sizing has been carried out according to the methodology presented in the following subsections.

2.2.1. Biological sizing

The biological sizing was carried out in order to determine the volume and surface area needed by the HRAPs to treat the wastewater according to the influent characteristics (Table 1) and flowrate. The main design parameter used to determine the surface area of the HRAPs was the organic loading rate (OLR), which represents the daily loading of organic matter per surface area of the HRAPs. To the authors' knowledge, there are no specific design criteria for HRAP, so they are usually designed as wastewater stabilization ponds. In such systems, the design is based on biological sizing based on the maximum amount of BOD_5 that can be removed per hectare and day. According to the experience in this field, 150 kg of $BOD_5 \cdot hectare^{-1} \cdot day^{-1}$ is considered as the maximum organic load than should be fed to a pond in order to allow for organic matter removal as well as nitrification and, depending on the pond configuration, denitrification. Effluent concentrations of less than 10 $mg \cdot L^{-1}$ of total nitrogen and 25 $mg \cdot L^{-1}$ of BOD_5 can be achieved with this criteria, which are within the European regulation limits [27,28,29]. Besides, it has been considered that the hydraulic retention time (HRT) should be at least 4 days, which has been previously proposed as the minimum for the biological processes to carry out the removal of nutrients and organic matter under optimal solar radiation and temperature [10,20].

The surface area of the HRAPs has been determined by the influent organic load and the maximum OLR, while the total volume has been determined by the influent flowrate and the minimum HRT.

The surface area can also be calculated from the total volume by considering a maximum depth of 0.3 m. Indeed, the water level in the HRAP has to be set around 0.3 m, in order to allow the penetration of solar radiation to the whole layer, reaching the bottom of the HRAPs [12]. These estimations were carried out according to Eq. (1) and (2), respectively.

Once the surface was calculated based on both parameters, the most restrictive (higher surface) result was chosen for the HRAPs design.

$$A = \frac{L_i}{OLR} \quad (1)$$

$$V = Q \times HRT \quad (2)$$

Where:

$A = \text{total surface area, ha}$

$L_i = \text{influent organic load, kg } BOD_5 \cdot day^{-1}$

$OLR = \text{maximum organic loading rate, kg } BOD_5 \cdot ha^{-1} \cdot day^{-1}$

$V = \text{total volume, } m^3$

$Q = \text{influent flowrate, } m^3 \cdot day^{-1}$

$HRT = \text{minimum hydraulic retention time, days}$

2.2.2. Hydraulic sizing

The flow regime in the HRAP should be turbulent in order to enhance vertical mixing, keep the biomass in suspension and facilitate the removal of the oxygen produced by photosynthesis. Indeed, an improper vertical mixing entails vertical stratification and uneven exposure of the biomass to the solar radiation causing photolimitation and photoinhibition. Moreover, if the biomass is not kept in suspension, biomass settling can cause biomass accumulation at the bottom of the HRAP, preventing proper fluid circulation and jeopardizing the appropriate collection of biomass in the subsequent harvesting process.

The turbulent conditions in a fluid flow through pipes can be guaranteed by keeping a Reynolds number (Re) higher than 4,000. However, in fluid flow through channels the transition from laminar to turbulent flow is not so clearly defined, so Re higher than 8,000 should be considered in open channels to guarantee turbulent conditions [12,30]. Re is directly proportional to the fluid velocity, the diameter of the flow conduit and the fluid density, and it is inversely proportional to the liquid viscosity (Eq. (3)). In channels, which are open, non-circular tubes, the diameter of the flow conduit is expressed by the hydraulic diameter dh [12,31], which is four times the cross-sectional area of the flow divided by the wetted perimeter of the cross-section (Eq. (4)).

$$Re = \frac{\rho \ v \ D}{\mu} \quad (3)$$

Where:
Re = Reynolds number (dimensionless)
v = average flow velocity ($m \cdot s^{-1}$)
D = diameter of the flow conduit (m)
ρ = density of the mixed liquor ($kg \cdot m^{-3}$)
μ = viscosity of the mixed liquor (Pa·s)

$$dh = \frac{4Wd}{W + 2d} \quad (4)$$

Where:
dh = hydraulic diameter
W = channel width
d = channel depth

According to [32] a velocity of around 0.1 $m \cdot s^{-1}$ is needed to prevent sedimentation of algal biomass. Therefore, a water velocity of 0.15 $m \cdot s^{-1}$ was set in the HRAPs presented in this study. In addition, the ratio length to width of the channel should be 10 or larger. For ratios smaller than 10, the flow in the straight parts the HRAP can be significantly affected by the disturbances caused by the reversals of the channel [33]. Indeed, the semi-circular ends or

reversals of the HRAPs promote the formation of dead zones and causes energy losses.

Another important hydraulic parameter to take into account in open channels is the Froude number (F_R), which relates the effect of the inertial forces to the gravity forces acting on the fluid according to Eq. (5).

$$F_R = \frac{v}{\sqrt{g \cdot D_H}} \quad (5)$$

Where:
g = acceleration due to gravity ($m \cdot s^{-2}$)
$D_H = \frac{A}{T}$ = Hydraulic depth (m)
A = cross-sectional area of the flow (m^2)
T = width of the channel water surface (m)

Values of F_R higher than 1 imply that the inertial forces acting on the flow are greater than the gravity forces, provoking a supercritical flow, which can lead to erosion and the formation of hydraulic jumps. If the rapidly flowing liquid is slowed increasing the depth of the channel, the flow can become subcritical ($F_R < 1$), converting part of the kinetic energy into potential energy, with some energy irreversibly lost through turbulence and heat release. Although these ridges would not present any major disadvantage for the microalgae culture, it could cause erosion and losses of the mix liquor sprinkling over the external walls of the channel. Therefore, F_R below 1 are desired.

Subsequently, the power of the paddlewheel required to generate a flow with the desired velocity has been determined according to Eq. (6). The power requirement is proportional to the flowrate of mixed liquor through the cross-section area of the HRAP (as shown in Eq. (7)), and the total head loss (Eq. (8)) was obtained by the sum of the head losses from the straight parts and reversals, which have been determined by the Manning equations as it is shown in Eq. (9) and Eq. (10), respectively.

$$P = \frac{Q\ \gamma\ \Delta h_d}{E} \quad (6)$$

$$Q = dWv \quad (7)$$

Where:
P = hydraulic power requirements (kW)
Q = flow the water in motion ($m^3 \cdot s^{-1}$)
γ = specific weight of water at 20 °C ($kN \cdot m^{-3}$)
Δh = total head loss (m)
E = Paddlewheel efficiency (dimensionless)

$$\Delta h_d = \Delta h_c + \Delta h_r \quad (8)$$

$$\Delta h_c = \frac{v^2 L}{\left(\frac{1.486}{n}\right)^2 \left(\frac{dW}{W+2d}\right)^{1.26}} \quad (9)$$

$$\Delta h_r = \frac{v^2}{2g} \quad (10)$$

Where:
Δh_c = head loss in the straight part of the HRAP (m)
Δh_r = head loss in the reversals of the HRAP (m)
L = Channel length (m)
g = gravitational acceleration ($m \cdot s^{-2}$)
n = Manning friction factor ($s \cdot m^{-1/3}$)

The efficiency of the paddlewheel is an important parameter, which is affected by the fluid leakage flowing backwards against the movement of the blades. During HRAP operation, the paddlewheel lifts the water up to the downstream side. This creates a head difference, which in turn drives backward flow through the gap between the paddles and the flat floor of the raceway, thus reducing the efficiency of the wheel. A higher number of blades reduces the fluid leakage and increases paddlewheel efficiency, while a higher rotating speed of the wheel increases the head difference and turbulence, reducing the efficiency. In addition, the space between the paddles and the floor of the raceway can be reduced by creating a crater under the paddlewheel. The crater curvature should match the path of the blades, thus reducing leakage. Specific studies have shown that an optimal design of the paddlewheel can increase the efficiency from 10% to 60% [34]. According to these considerations, the paddlewheels of the HRAPs presented in this manuscript were designed with 8 aluminium paddles, a gap of 2.5 cm between the paddles and the floor, and a crater of 10 cm depth and 1 m length. The efficiency used to estimate the required power was 30%, in order not to overrate the positive effects of the paddlewheel design. A detailed drawing of the paddlewheel is shown in Supplindeedementary Material (Fig. S3).

Note that the hydraulic power requirements (Eq. (5)) only refers to the energy needed for water flow, but not to the engine consumption, the type of wheel and the gearbox used, which are directly related to energy consumption. [34] reported that the total power required can be 5 times the calculated hydraulic power, which should be taken into account for the selection of the corresponding engines. The parameters used for the hydraulic sizing are shown in Table 3.

2.3. Mathematical models

Two mathematical models were used to simulate the operation of the HRAPs in order to verify and optimize the biological and hydraulic sizing and to better understand the system behaviour. On the one hand, the integral microalgae-bacteria biokinetic model BIO_ALGAE, developed by [20], was used to simulate the nutrients and organic matter removal and the biomass production. On the other hand, a 3D CFD model was used to comprehensively analyse the hydrodynamic behaviour of the system and to optimise the design of the HRAPs. Both models have been developed and implemented in COMSOL Multiphysics™ software.

2.3.1. Microalgal-bacteria biokinetic model

The integral microalgae-bacteria model BIO_ALGAE is based on the River Water Quality Model 1 (RWQM1) [35] and on the modified Activated Sludge Model ASM3 [36] of the International Water Association (IWA). The model uses the common nomenclature of the IWA models and considers 19 components implicated as variables in the physical, chemical and biokinetic processes. Among others, the BIO_ALGAE model includes nitrogen removal mechanisms such as microalgae and bacteria uptake, ammonia volatilization, nitrification and denitrification. Regarding phosphorus removal, uptake by microalgae and bacteria are considered. The effect of pH on other system variables, as well as the equilibrium between ammonia and ammonium according to the pH, are also considered in the model. Moreover, BIO_ALGAE includes the transfer of gases to the atmosphere, light attenuation, photorespiration and temperature dependency, and carbon limitation on the growth

Table 3
Set of parameters used for the hydraulic sizing of the HRAPs.

Parameter	Value
Water velocity (V), $m \cdot s^{-1}$	0.15
Water density (ρ), $Kg \cdot m^{-3}$	1,000
Water viscosity (μ), Pa·s	0.001
Specific weight of water at 20 °C (γ), $KN \cdot m^{-3}$	9.78
Manning friction factor (n), $s \cdot m^{-1/3}$	0.013
Gravitational acceleration (g), $m \cdot s^{-2}$	9.81
Channel depth (d), m	0.3
Hydraulic diameter (dh), m	1.043

of microalgae and autotrophic bacteria. The processes related to the storage of readily biodegradable soluble organic matter are not considered in the model. Due to the relatively oxidized nature of microalgal-bacterial processes, fermentation, sulphate reduction and other anaerobic biological processes were also omitted. And the absorption and desorption of phosphate on particulate matter were neglected.

Microalgae growth is expressed in the form of Monod functions with corrective factors which limit or inhibit their growth [37]. Microalgae grow with both carbon dioxide and bicarbonate [38] as carbon source and with ammonia and ammonium or with nitrate as nitrogen source [39,40]. Moreover, a photosynthetic factor depending on the light intensity and the oxygen excess also influences microalgae growth. Both factors were widely developed by [41] by means of 'Photosynthetic factories' model (PSF) and are included in the BIO_ALGAE model, including photolimitation and photoinhibition. The values of average monthly solar radiation obtained from [26] and shown in Table 2 have been distributed each day on an hourly basis according to the sun light intensity (which is related to the sun position from sunrise to sunset). The amount of solar radiation was converted to wavelength-specific irradiance, which is expressed as photon flux density (I(λ)) [μE $(m^2 \cdot s)^{-1}$] [42]. Moreover, the PAR radiation was used in the model simulations. PAR refers to the spectral range of solar radiation from 400 to 700 nm, which is used by photosynthetic microorganisms, expressed by Eq. (11), and it reaches approximately 45% of the total solar irradiation [43]. The maximum PAR at midday ranged between 921 (January) and 1302 (April) (Table 2).

$$PAR = \int_{400nm}^{700nm} I(\lambda) d\lambda \quad (11)$$

Microalgae growth also depends on the temperature, therefore a thermic photosynthetic factor was included in the model taking into account diurnal and seasonal variations [44]. In order to simulate the variable climatic conditions, a daily temperature cycle was also included with temperature oscillating from the average minimum to the average maximum of each month (Table 2) on an hourly basis [45].

A comprehensive description of the BIO_ALGAE model was previously reported in [20] and is included as Supplementary Material (Tables S3-S7). The model equations, which describe the processes and their rates, are shown in Table S1. Table S2 is the matrix of stoichiometric parameters. A complete list of parameters and stoichiometric coefficients used in the model are compiled in Tables S3–S5.

The BIO_ALGAE model was used to simulate the biological performance of the HRAPs. The simulations were performed time-dependent in order to reproduce the variable climatic conditions and wastewater characteristics. A period of 15 months was simulated in order to include the start-up period and a complete year of stable operation. The influent wastewater characteristics used in the simulations are the values shown in Table 1. The influent $P\text{-}PO_4^{3-}$ concentration was not available and was set at 4 $mg \cdot L^{-1}$, which is considered a typical value of untreated domestic wastewater [46]. In addition, the rainfall was included in the model causing a dilution of the influent wastewater and mixed liquor in the HRAP, in order to simulate the effect of rainwater in the system.

The initial concentrations of organic matter, total and volatile solids and nutrients within the HRAPs before wastewater feeding were set as follows: COD = 100 $mg \cdot L^{-1}$, TSS = 100 $mg \cdot L^{-1}$, VSS = 10 $mg \cdot L^{-1}$, $N\text{-}NH_4^+$=2 $mg \cdot L^{-1}$, $P\text{-}PO_4^{3-}$=0.5 $mg \cdot L^{-1}$. Such values have been estimated according to the authors' experience.

The performance of the HRAPs was simulated under four different operational conditions, modifying the HRT from 4 to 8 days, in order to compare the removal efficiencies and propose the best operational strategy. The variations of the HRT would be achieved by modifying the volume of the ponds, while keeping the same influent flowrate.

The parameters and constants included in the model have been taken from a previous calibration and validation of the BIO_ALGAE model, which was performed with experimental data from a set of three pilot HRAPs of 3.5 m^2 and 0.3 m deep located in California (USA), which were fed with municipal wastewater [20].

2.3.2. Hydrodynamic model

A 3D CFD model was used to simulate the hydrodynamic behaviour of different HRAP configurations in order to achieve a turbulent flow that ensures vertical mixing and thus avoid biomass sedimentation into the ponds. The conditions within the studied domain were carried out with the turbulent flow interface and considering stationary state. Turbulence was modelled by using the Reynolds averaged Navier-Stokes (RANS) equations. The standard k-ε two-equation turbulence model based on the turbulent kinetic energy (k) and the dissipation (ε) was implemented in the model.

The paddlewheel was simulated as an internal fan component, which was located at the same location of the paddlewheel and occupies the entire water cross section of the channel. The fan provided the desired mixed liquor velocity at that section.

The input data for model simulations were set according to the results obtained from the hydraulic sizing. The hydraulic domain of the different configurations was meshed with the COMSOL sequence type controlled by physics. The input data, k-ε model parameters and mesh characteristics used for the simulations of the hydrodynamic model are shown in Table 4.

The main objectives of the hydrodynamic model simulations were to analyse the velocity field in the HRAPs and to identify potential dead zones with low velocity. To this aim, 36 different HRAP designs were simulated and compared. The configurations were classified in three groups: reference group (GR), group A (GA) and group B (GB). The GR refers to HRAP with conventional carousel shape with a thickness of the central separation wall of 1/20 of the channel width. In the configurations of group A, the separation wall thickness was increased to 1/4, 1/2, 3/4 and 1/1 of the channel width in order to reproduce different shapes and curve diameters at the reversals. In group B, a tear-shape was included at the end of the central separation wall, with a diameter of 1/4, 1/2, 3/4 and 1/1 of the reversal width. In this way, the group B configurations aimed at reproducing the different shapes and curves diameters at the reversals, but reducing the volume occupied by the central separation wall in the HRAP. Finally, 1, 2 and 3 deflector baffles were included at the reversal of each configuration in order to compare and quantify the efficiency of the different combinations of these three components (increased wall thickness, tear-shape and deflector baffles).

In order to evaluate the hydrodynamic behaviour and land use efficiency of each configuration, three areas were defined: the total area occupied by the whole HRAP (A), the useless area occupied by the central separation wall, the tear-shapes and the deflector baffles (WTB), and the dead zones in the mixed liquor (DZ, determined as zones with velocity lower than 0.1 $m \cdot s^{-1}$). The hydrodynamic performance and land use efficiency were evaluated by determining the useless area ratio (U) as the percentage of useless area occupied by the separation wall, tear-shapes and deflector baffles, plus the dead zone area, out of the total area of the HRAP (Eq. (10)).

$$U = \frac{100(WTB + DZ)}{A} \quad (10)$$

2.4. Technical-economic assessment

A technical–economic assessment was carried out in order to estimate the power consumption and the implementation and

Table 4
Input data, parameters and main characteristics of the hydrodynamic model.

Input data	Value	k-ε parameter	Value	Mesh characteristics	Value
Water velocity	0.15 $m \cdot s^{-1}$	$C_{\varepsilon 1}$	1.44	**Number of elements**	48,071 – 87,730
Channel width	4 *m*	$C_{\varepsilon 2}$	1.92	**Average elements quality**	0.5171 – 0.5416
Water depth	0.3 *m*	$C\mu$	0.09	**Elements volume ratio**	0.02082 – $3.3 \cdot 10^3$
Density (ρ)	1,000 $kg \cdot m^{-3}$	σ_k	1	**Mesh volume**	126 – 144 m^3
Dynamic viscosity (μ)	1 cP	σ_k	1.3	**Number of vertex**	23,206 – 42,184
		κ_v	0.41	**Elements type**	Tetrahedral, pyramid, prism, triangle and quad
		B	5.2		

operation costs of the HRAPs, and to determine the main performance indicators. The costs considered in the study included the HRAP construction (components, materials and civil works), operation and maintenance (O&M) costs, hydraulic and electrical facilities and the biomass harvesting system. A Dissolved Air Flotation (DAF) unit was chosen to harvest the biomass and was dimensioned based on the biomass production estimated by model simulations. This technology was considered the most suitable process for the separation and harvesting of microalgae compared with sedimentation or centrifugation. Although sedimentation does not require aeration and has lower energy consumption, its efficiency is highly sensitive to seasonal variability in culture concentration and species. On the other hand, higher performance processes such as centrifugation or filtration were considered not suitable for wastewater treatment cultures, due to their high energy consumption and costs. Such technologies are only viable for closed cultures aiming to obtain high value products such as food, cosmetics, pigments, etc.

Note that the cost of microalgae treatment after harvesting was not considered in this study.

The implementation costs were obtained by CYPE price generator for civil works with the current European prices of mechanical and electrical devices (http://www.cype.com/en/).

For the O&M costs of the entire system, energy consumption and the maintenance works were considered. The energy consumption corresponds to the power consumptions of engines and pumps. The DAF are working 8 h per day at half of their maximum power, since it is oversized in order to provide the capacity to treat possible peak flows. The paddlewheel engines are working 24 h per day also at half of their capacity in order to increase their useful life.

The price of 0.2 $€ \cdot kWh^{-1}$ for electrical consumption was assumed according to the current average cost in Europe. For the maintenance works it was considered 2 h of personnel per week and 20 $€ \cdot h^{-1}$ in order to check the facilities and perform basic O&M operations.

Four performance indicators were determined in order to compare the feasibility and performance of the proposed system with other existing technologies: specific surface area ($m^2 \cdot PE^{-1}$) and specific investment cost ($€ \cdot PE^{-1}$) per population equivalent, and power consumption ($kWh \cdot m^{-3}$) and operating cost ($€ \cdot m^{-3}$) per m^3 of treated wastewater.

3. Results and discussion

3.1. Sizing of the HRAPs

3.1.1. Biological sizing

Considering the influent flowrate of 50 $m^3 \cdot d^{-1}$ and the minimum HRT of 4 days, the required volume of the HRAPs was 200 m^3. This total volume was divided into two identical HRAPs operating in parallel in order to have the possibility to compare different operation modes under the same weather conditions and wastewater characteristics. Moreover, two HRAPs allow for more flexibility in order to face possible operational problems.

The useful depth of the HRAPs was set to 30 cm, resulting in a surface area of 667 m^2 (333.5 m^2 each HRAP). To comply with the maximum value of 150 kg $BOD_5 \cdot ha^{-1} \cdot d^{-1}$, an area of 567 m^2 would be necessary. Therefore, the appropriate and proposed size for the HRAP was 667 m^2, which is the most restrictive, since otherwise the 4 days HRT requirement would not be fulfilled.

3.1.2. Hydraulic sizing

As shown in the materials and methods (section 2.2.2), the Re highly depends on the channel width. For the HRAPs of this study, it was set to 4 m, based on the area available at the site. Therefore, the total length of the raceway required to achieve the surface of each HRAP (333.5 m^2), including the reversals, was 86.2 m (two straight channels of 36.5 m and two reversals of 6.6 m).

The water velocity was set to 0.15 $m \cdot s^{-1}$ in order to prevent settling of the suspended solids (at velocities lower than 0.1 $m \cdot s^{-1}$). The Re of the flow with such velocity and the cited dimensions of the channel was 156,521, far above the limit to achieve a turbulent flow in open channels (8,000). On the other hand, with these conditions the F_R was 0.09, clearly below the critical value (F_R=1) that could promote hydraulic jump.

The head loss of the mixed liquor circulation through the HRAP was determined according to the parameters and variables shown in Table 3. The constructive material of the HRAPs in contact with the mixed liquor was PVC (Manning friction factor of 0.013 $s \cdot m^{-1/3}$). The total head loss was 0.5 cm, 0.3 cm corresponding to the straight parts of the channels and 0.2 cm corresponding to the reversals. Finally, the power of the paddlewheel required to overcome this head loss was 0.1 kW. As explained in section 2.2.2., this power only refers to the water flow, and this value was multiplied by 5 to establish the final energy requirement of the engines, i.e. 0.5 kW for the paddlewheel of each HRAP.

3.2. Simulation and optimization of the of biological performance

The BIO_ALGAE model was used to simulate the biological performance of the HRAPs in order to estimate the removal efficiency of nutrients and organic matter, the quality of the treated wastewater, the biomass production, and the start-up period required to achieve steady conditions.

The results of the simulations of the HRAPs operated at four different HRTs (4, 5, 6 and 8 days) are presented in Fig. 1. In all the configurations tested, the concentration of ammonium in the treated wastewater after the start-up period (around 1 month) was kept below 1 $mgN \cdot L^{-1}$, except during December and January for the configuration with HRT of 4 days (Fig. 1A). As expected, the higher the HRT, the lower the effluent ammonium concentration. The lower temperature and solar radiation in winter affected the removal of ammonium. Nevertheless, the effluent concentration was below 2 $mgN \cdot L^{-1}$ even in the simulation with the lowest HRT. The removal efficiency of ammonium ranged between 94% and 97%. The concentration of nitrate and nitrate resulted almost

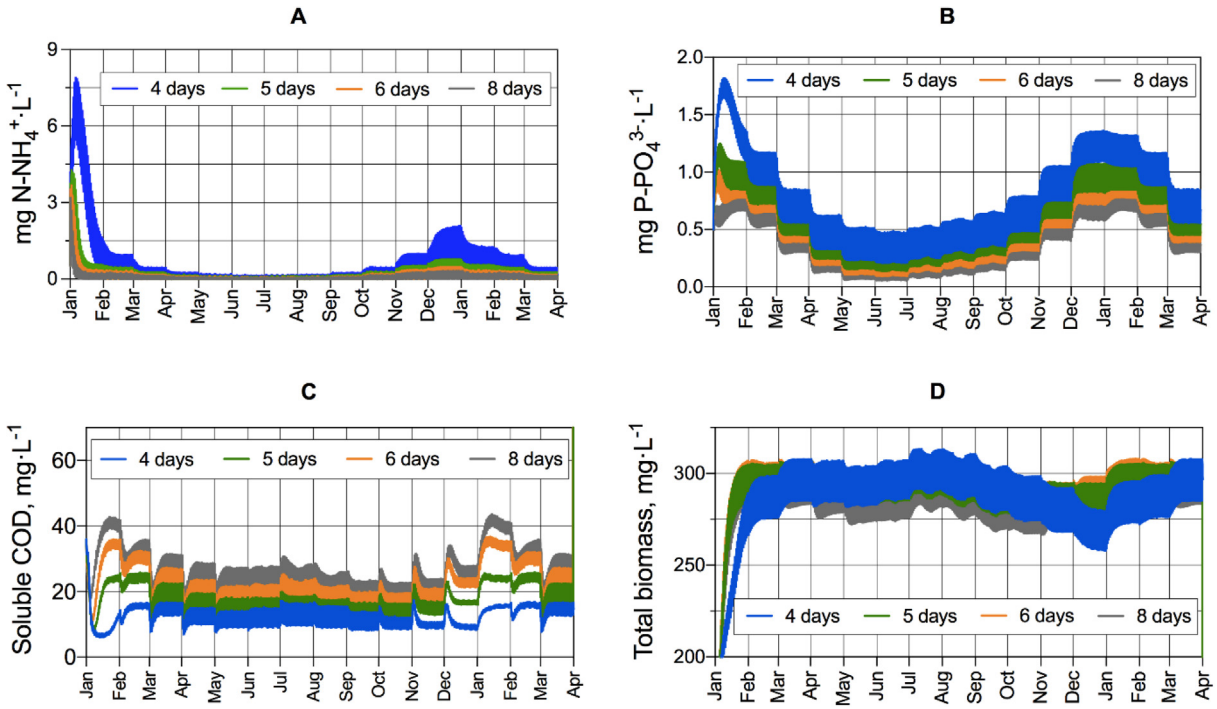

Fig. 1. Results of simulations performed with the BIO_ALGAE model for 4, 5, 6 and 8 days of HRT: (A) ammonium; (B) phosphate; (C) soluble COD concentration and (D) total biomass concentration in the HRAPs.

negligible, therefore the total nitrogen (sum of nitrate, nitrite and ammonium) increases up to 3 mg·L^{-1} in all cases. Such values are far below the maximum annual average of 15 mgN·L^{-1} required for the effluent of wastewater treatment plants in small populations discharging into sensitive areas (<100,000 population equivalent). Thus, an HRT of 4 days during the whole year is considered to be enough to achieve the desired effluent quality, regarding the concentration of total nitrogen.

The simulated concentration of phosphate in the treated wastewater was in all cases lower than 1.5 mgP·L^{-1}, apart from the start-up period (Fig. 1B). As in the case of ammonium, the higher the HRT, the lower the phosphate concentration. For the lowest HRT (4 days), phosphate concentration in the effluent ranged between 0.5 mg·L^{-1} from April to October and 1.4 mg·L^{-1} from November to March, which correspond to a removal efficiency of 90% and 65% in both periods, respectively. The more unfavourable weather conditions in winter hamper the removal of phosphorus. Taking into account that the maximum limit for phosphorus concentration discharged from treatment plants in small populations is 2 mg·L^{-1}, it could be advisable to increase the HRT to 5 days during winter, especially in December and January when the phosphate concentration is around 1.5 mg·L^{-1}, in order to guarantee the desired removal of phosphorus during the whole year.

Regarding the removal of organic matter, the simulated concentration of soluble COD in the effluent is shown in Fig. 1C. Differently to the concentration of nutrients, the concentration of soluble COD resulted higher in the simulations with higher HRT. This was attributed to the accumulation of biomass in the HRAP for longer periods of time, which would release soluble organic matter due to biomass decay and hydrolysis. The simulations predicted values around 30 mg·L^{-1}, which increased close to 50 mg·L^{-1} from December to March. These values are far from the 125 mg·L^{-1} limit of total COD required in the clarified effluent (after suspended solids separation and biomass harvesting). In particular, the concentration of soluble COD did not exceed 20 mg·L^{-1} in the simulations with HRT of 4 days, suggesting that the HRAPs perform satisfactorily with such HRT in terms of organic matter removal.

The biomass production was assessed in order to provide useful information for the design and operation of the subsequent harvesting unit, downstream processing and management of the biomass (which are out of the scope of the present study). The biomass concentration in the HRAPs, represented by the simulated concentration of total suspended solids (TSS), is presented in Fig. 1D for the different HRTs. The results showed a biomass concentration between 260 and 300 mgTSS·L^{-1} for every HRT and it suggests that HRTs above 4 days does not get a major increase of biomass concentration. However, for 4 days of HRT it was observed a decline of concentration below 260 mg·L^{-1} in December, but it was quickly recovered in January. Those values mean that the total biomass production ranged between 13 and 15 kg of TSS per day, which means 19.5–22.4 g·m^{-2}·d^{-1}, comparable to the value of 25 g·m^{-2}·d^{-1} reported by Chisti (2016) in well-operated raceways in sunny locations with stable and favourable diurnal temperature. Also, the annual average production of biomass per kWh·m^{-2} of PAR has been estimated. The hourly increase of TSS concentration was calculated and divided by the kWh of radiation received, resulting in 30.4 gTSS·(kWh PAR·m^{-2})$^{-1}$. In addition, if a solids concentration of 2% after the harvesting process is supposed (usually achievable with current harvesting processes and technologies), the produced biomass volume would be between 650 and 750 L per day (Fig. 1D).

Finally, regarding the start-up period, it can be observed in Fig. 1D that the steady concentration of biomass was achieved after 1 month of operation for the simulation with 4 days HRT, and only about 15 days for the simulations with 5, 6 and 8 days HRT. This start-up period coincides with the time required to achieve steady concentrations of nutrients and organic matter (Fig. 1A, 1B and 1C). This means that a period of about 1 month should be taken into account for the start-up of the process with the lowest HRT, and about half a month for the other scenarios. Note that the rainfall

on Monsoon period, from July to September, does not affect to the nutrient removal efficiency nor the biomass production.

This biokinetic model could be calibrated with experimental data once the plant is built and under operation, which could be used to confirm the reliability and validate the predictions of the model. This topic will be addressed in future research.

3.3. Simulation of the hydrodynamic conditions

Hydrodynamic simulations of the 36 HRAP configurations were performed in order to assess the hydraulic behaviour and optimize the design of the HRAPs. The 36 configurations refer to a HRAP with a total length of 86.2 m including 2 reversals in a carrousel shape. For the GR configurations (4), the channel width was 4 m and the central separation wall had a thickness of 1/20 the channel width. In GA configurations (16), the central separation wall thickness was increased in order to increase the curve diameter at the reversals, while keeping the channel width of 4 m. In GB configurations (16), tear-shapes were included at the ends of the central separation wall in order to increase the curve diameter in the reversals while keeping a thickness of the central separation wall of 1/20 the reversal width. These configurations aimed at maximizing the area and volume in the straight zones of the channel. The length of the tear-shapes was 8 m in all cases. In addition, all the configurations were simulated with 1, 2, 3 or without deflector baffles at the reversals.

The velocity fields of the 36 configurations are shown in Fig. 2, which were simulated at 15 cm height from the bottom. The results showed that in the designs without deflector baffles, the flow was clearly divided after the reversals into two sections with different velocities. A higher velocity zone was created close to the external wall of the HRAP, reaching values of 0.4 $m{\cdot}s^{-1}$, while a low velocity zone was located close to the central wall with velocities under 0.1 $m{\cdot}s^{-1}$. The latter is far below the desired 0.15 $m{\cdot}s^{-1}$. However, the increased thickness of the central wall in configurations GA had a positive effect, equalizing the velocity field and reducing the high and low velocity zones, as it can be observed in Fig. 2 (configurations GA $\frac{1}{2}$ 0, GA $\frac{3}{4}$ 0 and GA- $\frac{1}{1}$ 0).

The hydraulic behaviour improved significantly using a baffle at the reversals. In configurations GR and GA the high velocity zone disappeared, with a maximum velocity of 0.25 $m{\cdot}s^{-1}$, while the low velocity zone was reduced to a small area at the end of the central separation wall. Also, a small low velocity zone appears at the internal side of the baffle. However, in spite of the hydrodynamic improvement, in configurations GB there is still a low velocity zone close to the central separation wall, which is larger for larger diameters of the tear-shape.

When a second baffle is installed at the reversals, the low velocity zones are further reduced, almost disappearing in configurations GA. A small low velocity zone (<0.1 $m{\cdot}s^{-1}$) still remains at the end of the central separation wall in configurations GR and

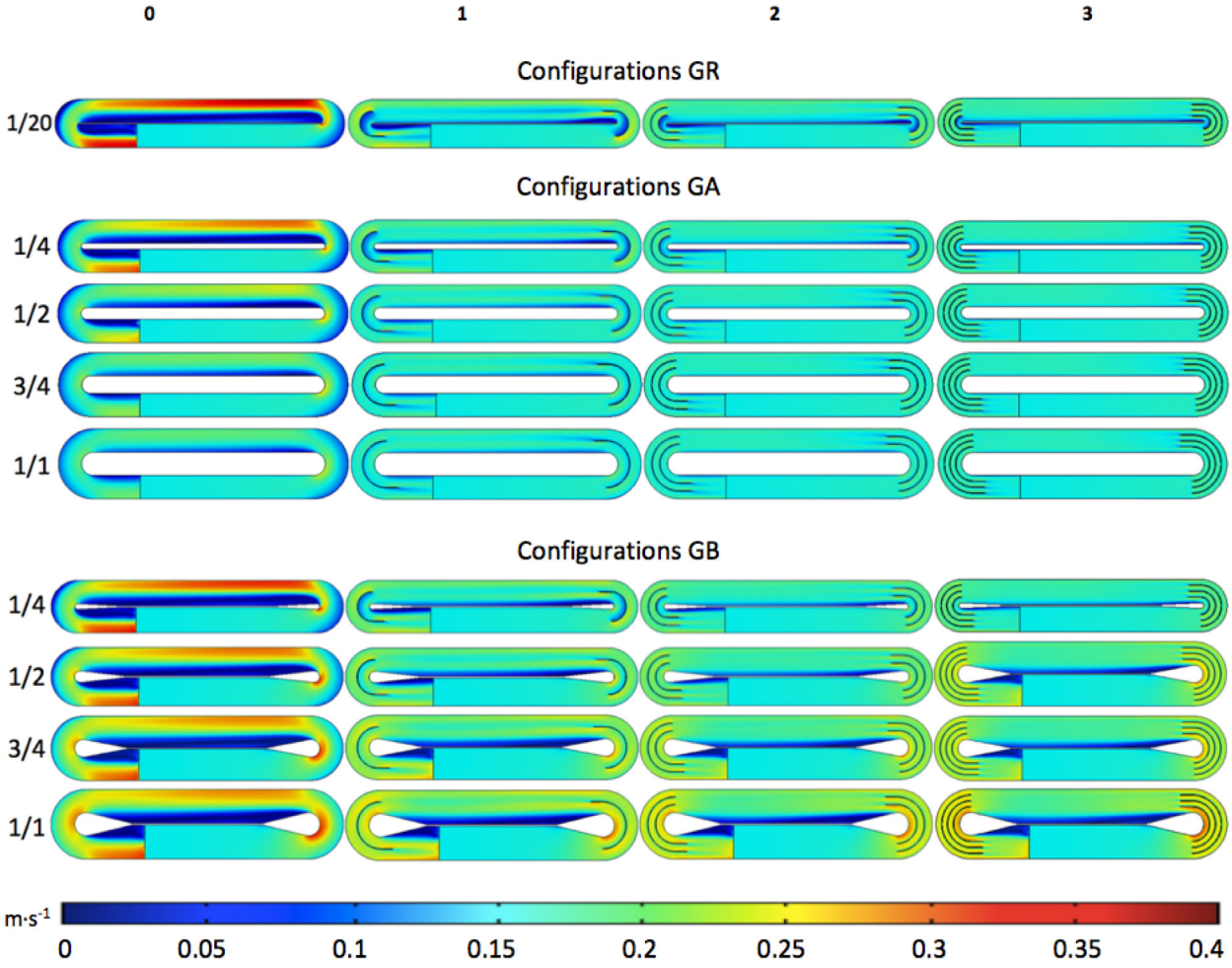

Fig. 2. Velocity fields of the 36 HRAP designs. Reference group (GR): central separation wall $\frac{1}{20}$ of the channel width. Group A (GA): central separation wall $\frac{1}{4}, \frac{1}{2}, \frac{3}{4}$ *and* $\frac{1}{1}$ (in rows) of the channel width. Group B (GB): tear-shapes at the end of the central separation wall with diameter $\frac{1}{4}, \frac{1}{2}, \frac{3}{4}$ *and* $\frac{1}{1}$ (in rows) of the reversal width. Each configuration was simulated with 0, 1, 2 and 3 deflector baffles at the reversals (in columns).

GB with the smallest tear-shape diameter. Moreover, low velocity zones are present in the GB configurations with the largest tear-shape diameters, together with high velocity zones at the reversals (up to 0.25 $m \cdot s^{-1}$). Finally, the addition of a third deflector baffle did not show significant improvement or difference in the hydrodynamic behaviour compared to the configurations with two deflector baffles.

In addition to the qualitative evaluation of the hydrodynamic behaviour, the hydrodynamic and land use efficiency of each configuration was quantified by determining the percentage of useless area. As described in the materials and methods section (2.3.2), the useless ratio U was defined as the percentage of useless area occupied by the separation wall, tear-shapes and deflector baffles, plus the low velocity area, out of the total area of the HRAP. Three-dimensional surface plots of U for each configuration, combining the different HRAP geometries and number of deflector baffles, are shown in Fig. 3. The U ratio of the configurations GA are presented in the left, and those for configurations GB in the right, both of them compared to configurations GR as a reference (1/20).

The results showed that in configurations GA, in spite of the clear hydrodynamic behaviour improvement due to the reduction of the low velocity zones, the increase of the thickness of the separation wall had a significant detrimental effect on the land use efficiency. The useless area occupied by the large central separation wall was significantly higher than the benefit caused by the reduction of low velocity zones, resulting in an increase of the U ratio in all the simulated configurations.

From the designs without deflector baffles at the reversals, which had high percentage of useless area values ranging from 34% (for GA $\frac{1}{4}$ 0) to 46% (for GA $\frac{1}{1}$ 0), the results improved using one deflector baffle to 19% (for GA $\frac{1}{4}$ 1) and 34% (for GA $\frac{1}{1}$ 1). This improvement decreased the U ratio between 11% and 16% for each design. Using two deflector baffles, the useless area further decreased between 2% and 5%, obtaining values from 14% (for GA $\frac{1}{4}$ 2) to 32% (for GA $\frac{1}{1}$ 2). The configurations with three deflector baffles did not show an improvement of the useless area. Indeed, there was an increase of 4% for GA $\frac{1}{4}$ 3, which means that there was no reduction of the low velocity zones, while the area occupied by the baffles was increased. GA $\frac{1}{4}$ 2 was the GA configuration with the lowest U ratio (14%), but still higher than the one of the reference configuration GR $\frac{1}{20}$ 2 (9%). Both configurations are shown more in detail in Fig. 4.

GA configurations showed to be very efficient with only one deflector baffle and even without deflector baffles. However, it can be concluded that the improvement of the hydrodynamic behaviour by increasing the thickness of the central wall requires a large land occupation. This configuration could be considered in cases in which there is no limitation of land availability, while it is not a suitable solution for locations with limited land availability. One possibility to take advantage from this configuration could be to make use of the area of the central separation wall, for instance to implement the harvesting unit or downstream processes, or a photovoltaic solar system for local production of renewable energy.

Regarding the configurations GB, simulations showed that the U ratio was significantly reduced compared to configurations GA for almost all the cases. The tear-shape at the end of the central separation wall proved to be useful to improve the hydrodynamics in the reversals while keeping a high culture volume. This is consistent with previous research performed by [14].

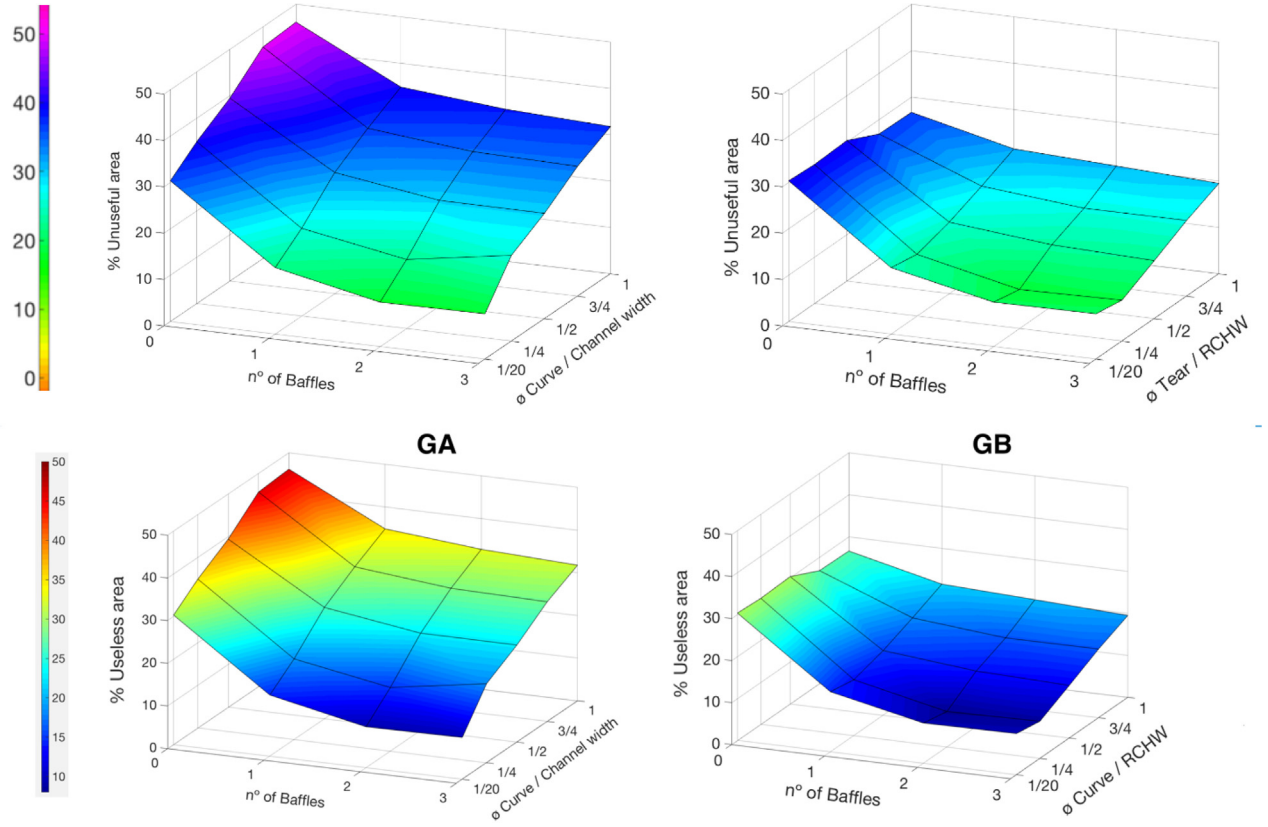

Fig. 3. Percentage of useless area (separation wall, tear-shapes and baffles, and low velocity zones) out of the total area of the HRAP for each combination of number of baffles and thickness of the separation wall (TSW) / channel width (configurations GA, left), and number of baffles and diameter of the tear-shape / reversal channel width (RCHW) (configurations GB, right). The reference configurations (GR, 1/20) are included in both plots.

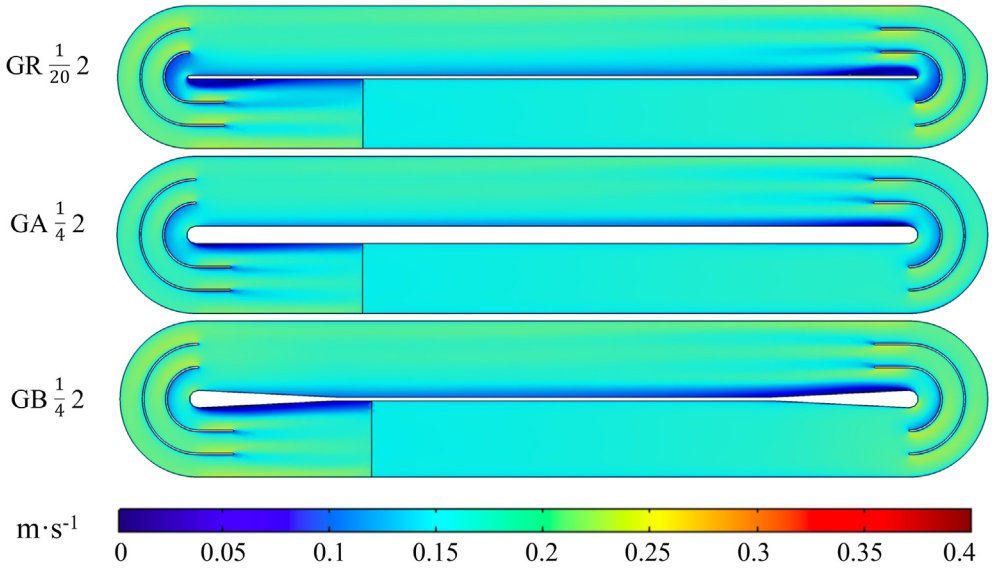

Fig. 4. Velocity fields of selected configurations with the lowest useless area: GA $\frac{1}{4}$ 2, GR $\frac{1}{20}$ 2 and GB $\frac{1}{4}$ 2 with U ratio of 14%, 9% and 8%, respectively.

For GB designs without deflector baffles, the U values were stable around 30% independently of the curve diameter. However, for designs with 1, 2 or 3 deflector baffles it can be observed a decrease of the U ratio with the tear diameter of ¼, and a trend of increasing U ratio with increasing tear diameter, as in GA. The U ratio reached a maximum close to 20% for curve diameters of $\frac{1}{1}$. The most efficient GB configurations were those with a diameter curve of $\frac{1}{4}$ and at least one baffle. In particular, the most efficient GB configuration was GB $\frac{1}{4}$ 2, achieving a U ratio of 8%, ranking as the lowest value obtained for all the simulated configurations, as can be observed in Fig. 3. This value was close to the one obtained with the reference configuration GR $\frac{1}{20}$ (9%). Note that in GR $\frac{1}{20}$ 2 the useless area was mainly located in low velocity zones at the ends of the central separation wall and the internal baffle. However, in GB $\frac{1}{4}$ 2 the main useless area was the area occupied by the tear-shapes, which in turn improves the hydrodynamic behaviour, favouring the flow between the tear and the internal baffle and removing the dead zone in this area. Nevertheless, for tear-shape diameter higher than $\frac{1}{2}$, the cross-section for mixed liquor circulation through the curves became too narrow compared to the channel width and results in the formation of high velocity zones. That velocity difference resulted in a low velocity zone close to the central separation wall in all configurations, even using 1, 2 or 3 deflector baffles. The detailed velocity field of configuration GB1/4 2 is shown in Fig. 4, together with configurations GR1/20 2 and GA1/4 2. It can be concluded that the implementation of tear-shapes at the end of the central separation wall improves the hydrodynamic performance in an efficient way from the point of view of land utilization, whilst an excessive diameter of the tear-shapes has a detrimental effect in the hydrodynamic behaviour.

4. Final HRAPs design and layout

According to the results of the preliminary sizing, the simulations of the biokinetic and hydrodynamic models, and the available area at the site, the design of the HRAP resulted in two equal HRAPs working in parallel, with total dimensions of 50 m length and 17 m width. The two HRAPs had a total area of 667 m^2 and volume of 200 m^3 required to treat a daily wastewater volume of 50 m^3 (25 $m^3 \cdot d^{-1}$ each HRAP). Such design, consisting of two HRAPs, was proposed in order to increase the flexibility of the operation and maintenance, as well as for research purposes, giving the opportunity to study different scenarios of OLR, HRT and other operational parameters in the two HRAPs under the same climatic conditions. The chosen configuration for both HRAPs was the one with tear-shapes at the ends of the central separation wall with a diameter ¼ times the channel width and 2 deflector baffles (GB $\frac{1}{4}$ 2). This configuration showed a good hydrodynamic behaviour and the lowest U ratio, so it was selected in order to minimize the land occupation and to maximize the useful area available for the microalgae culture and wastewater treatment. A detailed 3D representation of the HRAPs is shown in Fig. 5. More details and drawings of the two HRAPs and reversals are shown in supplementary material (Figs. S1 and S2). The inlet was located just before the paddlewheel to achieve a good mixing (Fig. S5). The effluent from each HRAPs was collected by means of two notch-weirs at different levels in order to allow the selection of two different water levels inside the HRAPs. One of them was set at 30 cm to operate the HRAPs with 4 days of HRT, which is proposed for usual climatic conditions. The second notch was set at 40 cm, which is intended to increase the HRT up to 5 days if needed during unfavourable climatic conditions periods. This option will only be considered during limited periods of time characterized by specific climate conditions (winter). Note that a recent study showed similar performances in terms of biomass production and nutrients removal in HRAPs of 30 and 40 cm depth [47]. Downwards the

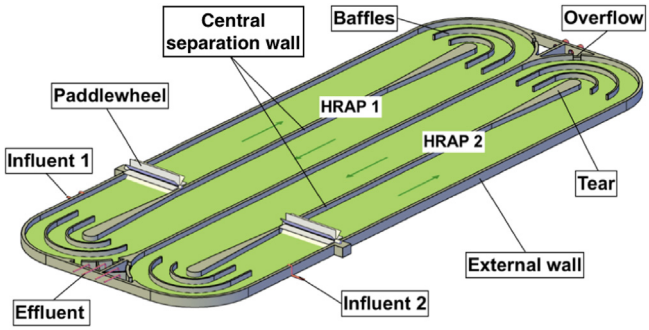

Fig. 5. 3D representation of the two HRAPs: 45 m total length, 17 m total width, 4 m channel width, two baffles at reversals and tear-shape with curve diameter of ¼ times the channel width.

notch-weirs of each HRAP, the effluent is collected in two small basins (Fig. S6) from which it is pumped by automatic submersible pumps to the harvesting unit. This was done in order to keep the water level of collection basins always below level of the notch. In order to prevent the HRAP from flooding and overflow due to emergency situation as failure of the effluent, collection pumps or unexpected strong rains, an overflow collection system was included, consisting into two notch-weirs at 50 cm and collection basins connected to the drainage system (Fig. S7).

The outer walls, central separation walls, baffles and tear-shapes were designed to be constructed with cavity concrete blocks (39x19x19 cm) on top of 35 cm of cleaning concrete base. A plasticized polyvinyl chloride (PVC-P) waterproof layer covers the previous compacted soil and the constructed structure. Each paddlewheel is divided in two sections in order to avoid excess bending stresses and it is supported by three reinforcement concrete supports each. A detail construction drawing is shown in Fig. S4 of the supplementary material.

The HRAPs has to be fed with 50 m^3 in daytime conditions. Therefore, the workflow is actually between 4–7 $m^3 \cdot h^{-1}$. As a result, a Dissolve Air Flotation system (DAF) was set with a capacity suitable to treat that effluent.

5. Techno-economic assessment

A techno-economic assessment of the demonstrative scale HRAP system was performed in order to estimate the implementation and operating costs, the power consumption, and to determine the main techno-economic performance indicators.

The investment cost of the treatment system has been organized into five sections: HRAP construction, hydraulic facilities, electrical facilities, paddlewheels, and harvesting system. The detailed costs of these section are presented in Table S15, and a summary of the contribution of each section to the total implementation cost is shown in Fig. 6. The main cost turns out to be the harvesting unit (DAF) accounting for more than 44.9 % of the total cost. While the waterproof layer is 18.9 % and the paddlewheel implementation is 15 %. The pond constructions and the electrical facilities account for only 10.5 and 7.8 % respectively of the total implementation cost.

The power consumption was estimated taking into account the power of all electrical appliances and their operation time, including pumps, paddlewheels and DAF system. While the pumps and the paddlewheels accounted for 14 % and 18 %, respectively, the DAF system reached 36 % of the total power consumption. These values show that the biomass harvesting is the process that consumes the most.

The operating cost was estimated considering the expenses for power consumption and the personnel cost for maintenance works. The power consumption accounted for 40 % of the total operating cost, giving as a result 0.076 €·m^{-3} (Table S2 of supplementary material). The remaining 60 % corresponded to the personnel cost (0.114 €·m^{-3}), which can be positively considered as a green job. These values were compared with those of other technologies reported in other studies, and are summarized in Table 5. The resulting percentages obtained in the HRAP contrast with the average operation costs of different small municipal wastewater treatment plants (MWTP) (75 % extended aeration plants) presented in [48], in which the power consumption achieved 62.5 % and the personnel cost was 37.5 %. A similar study reported the costs of four wastewater treatment technologies: conventional activated sludge (CAS), extended aeration (EA), sequencing batch reactors (SBR) and aerated lagoon (AL) [49]. The resulting percentages of power consumption cost and personnel cost ranged between 53 and 68 % and 32–47 %, respectively. The values also differ from the results of the HRAP, in which the personnel cost is higher. This fact can be attributed to the low power consumption of the HRAPs technology. However, a study carried out by [50], which studied the cost of constructed wetlands (CW) operation, showed a lower power consumption cost (24 %). The reason for this difference can be attributed to the extremely low energy requirements of CW operation, which consist only in the influent pumping, compared to the use of a paddlewheel in the HRAPs, which implies and extra power demand.

Furthermore, the specific operation costs (including both power consumption and personnel) per PE and year of the references mentioned above have been compiled and compared with the present study (Table 5). A specific cost of 16.3 €·$PE^{-1} \cdot yr^{-1}$ was estimated for the HRAP. This value is within the small municipal treatments plants (mainly extended aeration technology for less than 10,000 PE) analysed by [48], which ranged between 12.8 and 17.0 €·$PE^{-1} \cdot yr^{-1}$. However, the operations cost of the constructed wetlands presented by [50] were far below of the HRAP ones (6.9 €·$PE^{-1} \cdot yr^{-1}$ for PE = 1000). The lack of electromechanical equipment, coupled with the low maintenance requirements of this technology, results in a low power consumption and personnel demand. On the other hand, the compiled operational costs by [49] of four wastewater treatment technologies at full-scale (>15,000 PE) were considered for comparison. The operation cost of the HRAP was within the range of those obtained with extended aeration system (7.3–23.0 €·$PE^{-1} \cdot yr^{-1}$) and close to the

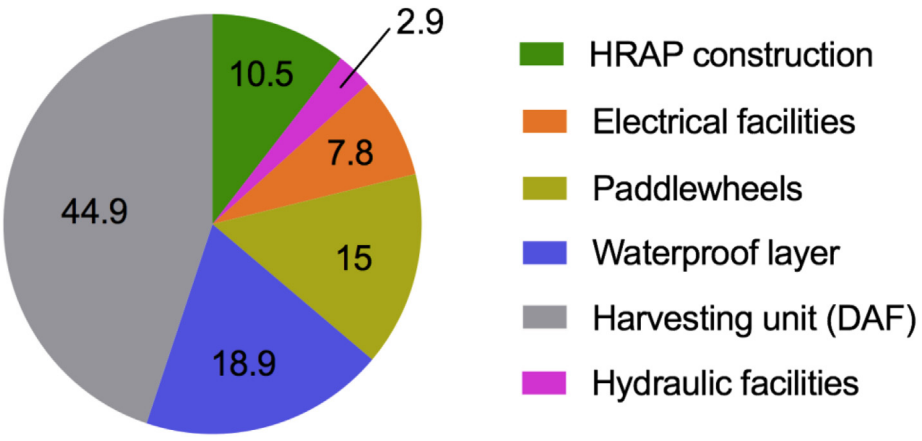

Fig. 6. Summary of the contribution of each section to the implementation cost (percentage of the total cost).

Table 5
Comparison between power consumption and personnel cost of different wastewater treatment technologies for small populations. HRAP: high rate algal pond; CW: constructed wetland; MWTP: small municipal wastewater treatment plant; CAS: conventional activated sludge; EA: extended aeration; SBR: sequencing batch reactor; AL: aerated lagoon.

Technology	PE	Power cost (%)	Personnel cost (%)	€·PE^{-1}·yr^{-1}	Reference
HRAP	212	40	60	16.3	This study
CW	1,000	24	76	6.9	[50]
MWTP	<10,000	62.5	37.5	12.8–17.0	[48]
CAS	>15,000	68	32	3.4–6.4	[49]
EA		54	46	7.3–23.0	
SBR		53	47	5.8–11.4	
AL		59	41	12	

aerated lagoon (12 €·PE^{-1}·yr^{-1}), but far from the conventional activated sludge (3.4–6.4 €·PE^{-1}·yr^{-1}) and sequencing batch reactors systems (5.8–11.4 €·PE^{-1}·yr^{-1}). The higher size of these technologies (>15,000 PE) compared to the HRAP (212 PE) can cause a better economic efficiency and therefore a lower specific cost, so this comparison cannot be considered decisive. As a result of HRAP sizing and the techno-economic evaluation presented in this section, the main performance indicators have been calculated and are presented in Table S2. The specific surface area occupied by the system is 3.1 m^2·PE^{-1}, which is slightly lower of the land requirement of other natural technologies for wastewater treatment at this scale, such as horizontal flow constructed wetlands, sand filters, infiltration, peat filters and waste stabilization ponds [51]. The specific investment cost is 483 €·PE^{-1}, which is in the range of the cost reported by Moragas (2012) or small treatment systems of about 400 PE with different technologies, from 385 to 850 € per PE. The power consumption per m^3 of treated wastewater reached 0.38 kWh·m^{-3}, which is in the range of power consumption of natural technologies for wastewater treatment, and lower to the energy requirement of conventional activated sludge systems [52]. Finally, the operating cost per m^3 of treated wastewater is 0.19 €·m^{-3}, which is within the range of operating cost of large scale conventional wastewater treatment (0.1–0.3 €·m^{-3}) [53,54]. It should be highlighted that this range refers to large wastewater treatment plants (>10,000 PE), in which the specific costs are usually reduced compared to small plants. In addition, the harvested microalgae biomass can be valorised as bioproducts or bioenergy, which can lower the cost to a greater or lesser extent depending on the final product.

6. Conclusions

In this study, advanced biokinetic and hydrodynamic modelling have been used to assist, verify and optimize the design of a full-scale microalgae-based wastewater treatment system. The system, which is being built in Aligarh (India), consists in two HRAPs. The models allowed to simulate the biological performance under different operational conditions and the hydrodynamic behaviour of different HRAP design and configurations.

Biokinetic simulations showed suitable removal rates of nitrogen and organic matter with an HRT of 4 days, with the wastewater characteristics and climatic conditions of Aligarh. The simulations also showed that the phosphate removal was close to the desired level during winter period, with a descent of temperature and solar radiation. This led to include the possibility of increasing the HRT from 4 to 5 days in the design, in order to guarantee the desired effluent quality during this climatic period. Hydrodynamic simulations showed that the hydrodynamic behaviour improved when one or two deflector baffles were added in the reversals, while the addition of a third one did not show a significant positive effect. HRAP configurations with increased thickness of the central separation wall could also improve the hydrodynamic behaviour. However, it requires a large land occupation due to the increase of the useless area of the HRAP layout. Finally, the implementation of tear-shapes at the end of the central separation wall improved the hydrodynamic performance in an efficient way from the point of view of land utilization. An excessive diameter of the tear-shapes could have a detrimental effect in the hydrodynamic behaviour; hence, a configuration with two deflector baffles and a diameter of the tear-shapes of ¼ of the channel width was selected. A techno–economic assessment showed that the HRAP can be implemented at this scale at a cost of 483 € per population equivalent with an operating cost of 0.19 € per m^3 of treated wastewater.

CRediT authorship contribution statement

Antonio Ortiz: Conceptualization, Investigation, Writing – original draft. **Rubén Díez-Montero:** Conceptualization, Writing – original draft, Visualization, Writing – review & editing. **Joan García:** Investigation, Visualization, Funding acquisition, Writing – review & editing. **Nadeem Khalil:** Visualization, Writing – review & editing. **Enrica Uggetti:** Conceptualization, Funding acquisition, Writing – review & editing.

Declaration of Competing Interest

The authors declare that they have no known competing financial interests or personal relationships that could have appeared to influence the work reported in this paper.

Acknowledgments

Authors would like to thank the European Commission for the financial support (PAVITR project, GA 821410) and the Department of Sciences and Technology from Government of India for the financial support (GA DST/IMRCD/India-EU/Water Call2/PAVITR/2018). Authors are also grateful to the Government of Catalonia (Consolidated Research Group 2017 SGR 1029). E. Uggetti and R. Díez-Montero would also like to thank the Spanish Ministry of Industry and Economy for their research grants (RYC2018-025514-I and IJC2019-042069-I, respectively).

Appendix A. Supplementary data

Supplementary data to this article can be found online at https://doi.org/10.1016/j.csbj.2021.12.034.

References

[1] García J, Ortiz A, Álvarez E, Belohlav V, García-Galán MJ, Díez-Montero R, et al. Nutrient removal from agricultural run-off in demonstrative full scale tubular photobioreactors for microalgae growth. Ecol Eng 2018;120:513–21. https://doi.org/10.1016/j.ecoleng.2018.07.002.

[2] Rueda E, García-Galán MJ, Ortiz A, Uggetti E, Carretero J, García J, et al. Bioremediation of agricultural runoff and biopolymers production from cyanobacteria cultured in demonstrative full-scale photobioreactors. Process Saf Environ Prot 2020;139:241–50. https://doi.org/10.1016/j.psep.2020.03.035.

[3] Khan MI, Shin JH, Kim JD. The promising future of microalgae: Current status, challenges, and optimization of a sustainable and renewable industry for biofuels, feed, and other products. Microb Cell Fact 2018;17(1):1–21. https://doi.org/10.1186/s12934-018-0879-x.
[4] Arashiro LT, Ferrer I, Pániker CC, Gómez-Pinchetti JL, Rousseau DPL, Van Hulle SWH, et al. Natural Pigments and Biogas Recovery from Microalgae Grown in Wastewater. ACS Sustain. Chem. Eng. 2020;8(29):10691–701. https://doi.org/10.1021/acssuschemeng.0c01106.
[5] Marín D, Ortíz A, Díez-Montero R, Uggetti E, García J, Lebrero R, et al. Influence of liquid-to-biogas ratio and alkalinity on the biogas upgrading performance in a demo scale algal-bacterial photobioreactor. Bioresour Technol 2019;280:112–7. https://doi.org/10.1016/j.biortech.2019.02.029.
[6] R. Díez-Montero *et al.*, "Scaling-up the anaerobic digestion of pretreated microalgal biomass within a water resource recovery facility," vol. "in press," 2020.
[7] Li K, Liu Q, Fang F, Luo R, Lu Q, Zhou W, et al. Microalgae-based wastewater treatment for nutrients recovery: A review. Bioresour Technol 2019;291:121934. https://doi.org/10.1016/j.biortech.2019.121934.
[8] Park JBK, Craggs RJ. Wastewater treatment and algal production in high rate algal ponds with carbon dioxide addition. Water Sci Technol 2010;61(3):633–9. https://doi.org/10.2166/wst.2010.951.
[9] Acién FG, Gómez-Serrano C, Morales-Amaral MM, Fernández-Sevilla JM, Molina-Grima E. Wastewater treatment using microalgae: how realistic a contribution might it be to significant urban wastewater treatment? Appl Microbiol Biotechnol 2016;100(21):9013–22. https://doi.org/10.1007/s00253-016-7835-7.
[10] Deb UK, Shahriar M, Bhowmik J, Chowdury MKH. The Effect of Irradiance Related Temperature on Microalgae Growth in a Tubular Photo Bioreactor for Cleaner Energy. Am. J. Comput. Math. 2017;07(03):371–84. https://doi.org/10.4236/ajcm.2017.73026.
[11] Arcila JS, Buitrón G. Influence of solar irradiance levels on the formation of microalgae-bacteria aggregates for municipal wastewater treatment. Algal Res. 2017;27(March):190–7. https://doi.org/10.1016/j.algal.2017.09.011.
[12] Chisti Y. Raceways-based production of algal crude oil. Green 2013;3(3–4):195–216. https://doi.org/10.1515/green-2013-0018.
[13] Sompech K, Chisti Y, Srinophakun T. Design of raceway ponds for producing microalgae. Biofuels 2012;3(4):387–97. https://doi.org/10.4155/bfs.12.39.
[14] Hadiyanto H, Elmore S, Van Gerven T, Stankiewicz A. Hydrodynamic evaluations in high rate algae pond (HRAP) design. Chem Eng J 2013;217:231–9. https://doi.org/10.1016/j.cej.2012.12.015.
[15] J. Climent, L. Basiero, R. Martínez-Cuenca, J. G. Berlanga, B. Julián-López, and S. Chiva, "Biological reactor retrofitting using CFD-ASM modelling," *Chem. Eng. J.*, vol. 348, no. June 2017, pp. 1–14, 2018, doi: 10.1016/j.cej.2018.04.058
[16] Arnaldos M, Rehman U, Naessens W, Amerlinck Y, Nopens I. Understanding the effects of bulk mixing on the determination of the affinity index: Consequences for process operation and design. Water Sci Technol 2018;77(3):576–88. https://doi.org/10.2166/wst.2017.550.
[17] Castrillo M, Díez-Montero R, Esteban-García AL, Tejero I. Mass transfer enhancement and improved nitrification in MABR through specific membrane configuration. Water Res 2019;152:1–11. https://doi.org/10.1016/j.watres.2019.01.001.
[18] Blanco-Aguilera R, Lara JL, Barajas G, Tejero I, Díez-Montero R. Hydrodynamic optimization of multi-environment reactors for biological nutrient removal: A methodology combining computational fluid dynamics and dimensionless indexes. Chem Eng Sci 2020;224:115766. https://doi.org/10.1016/j.ces.2020.115766.
[19] Bernard O, Mairet F, Chachuat B. Modelling of microalgae culture systems with applications to control and optimization. Adv Biochem Eng Biotechnol 2015;153:59–87. https://doi.org/10.1007/10_2014_287.
[20] Solimeno A, Parker L, Lundquist T, García J. Integral microalgae-bacteria model (BIO_ALGAE): Application to wastewater high rate algal ponds. Sci Total Environ 2017;601–602:646–57. https://doi.org/10.1016/j.scitotenv.2017.05.215.
[21] Sawant SS, Gosavi SN, Khadamkar HP, Mathpati CS, Pandit R, Lali AM. Energy efficient design of high depth raceway pond using computational fluid dynamics. Renew. Energy 2019;133:528–37. https://doi.org/10.1016/j.renene.2018.10.016.
[22] J. A. Álvarez *et al.*, "Constructed wetlands and solar-driven disinfection technologies for sustainable wastewater treatment and reclamation in rural India: SWINGS project," *Water Sci. Technol.*, vol. 76, no. 6, pp. 1474–1489, 2017, doi: 10.2166/wst.2017.329
[23] Kulshrestha K, Khalil N. Performance Assessment of the Vertical Flow Constructed Wetlands Treating Effluent from the UASB Reactor – A Demonstration in a Tropical Climatic Region. Int. J. Recent Technol. Eng. 2019;8(4):9779–81. https://doi.org/10.35940/ijrte.d2378.118419.
[24] Henze M, Harremoës P, Jansen J, Arvin E. Wastewater treatment: Biological and Chemical Processes. 3rd ed. Berlin/Heidelberg, Germany: Environmental Engineering Series; 2002.
[25] Mara D. Domestic Wastewater Treatment in Developing Countries. London: Earthscan; 2003.
[26] E. Kumar, D. Boruah, R. R. Guru, A. Verma, B. Laasya, and S. Saikia, "Development of Agra Solar City," New Delhi, 2011.
[27] *European Union (1991). Council Directive 91/271/EEC of 21 May 1991 concerning urban wastewater treatment. Official Journal L 135 30/05/1991, 0040–0052.*
[28] Matamoros V, Gutiérrez R, Ferrer I, García J, Bayona JM. Capability of microalgae-based wastewater treatment systems to remove emerging organic contaminants: A pilot-scale study. J Hazard Mater 2015;288:34–42. https://doi.org/10.1016/j.jhazmat.2015.02.002.
[29] Gutiérrez R, Ferrer I, Uggetti E, Arnabat C, Salvadó H, García J. Settling velocity distribution of microalgal biomass from urban wastewater treatment high rate algal ponds. Algal Res. 2016;16:409–17. https://doi.org/10.1016/j.algal.2016.03.037.
[30] Post S. Applied and Computational Fluid Mechanics. Jones & Bartlett Learning 2011.
[31] Perry S, Perry RH, Green DW, Maloney JO. Perry's chemical engineers' handbook 1997.
[32] Y. Chisti, "Algae biotechnology, Green Energy and Technology.," in *Algae Biotechnology, Green Energy and Technology*, 2016, pp. 21–40.
[33] F. Bux and Y. Chisti, "Algae biotechnology. Products and processes," *Green Energy Technol.*, no. March, p. 344, 2016, doi: 10.1007/978-3-319-12334-9.
[34] Musgrove E, Heaven S, Muller G. Investigating the performance of paddlewheels used in microalgae raceways for the production of biomass. University of Southampton; 2017.
[35] P. Reichert *et al.*, "River Water Quality Model no. 1 (RWQM1): II. Biochemical process equations," *Water Sci. Technol.*, vol. 43, no. 5, pp. 11–30, 2001, doi: 10.2166/wst.2001.0241
[36] Iacopozzi I, Innocenti V, Marsili-Libelli S, Giusti E. A modified Activated Sludge Model No. 3 (ASM3) with two-step nitrification-denitrification. Environ. Model. Softw. 2007;22(6):847–61. https://doi.org/10.1016/j.envsoft.2006.05.009.
[37] Monod J. The Growth of Bacterial Cultures. Annu Rev Microbiol 1949;3(1):371–94. https://doi.org/10.1146/micro.1949.3.issue-110.1146/annurev.mi.03.100149.002103.
[38] H. J. Silva and J. Print, "Carbon dioxide inhibition of photosynthetic growth of chlorella," pp. 2833–2838, 1984, [Online]. Available: https://doi.org/10.1099/00221287-130-11-2833.
[39] Mostert ES, Grobbelaar JU. The influence of nitrogen and phosphorus on algal growth and quality in outdoor mass algal cultures. Biomass 1987;13(4):219–33. https://doi.org/10.1016/0144-4565(87)90061-8.
[40] P. J. Syrett, "Nitrogen Metabolism of Microalgae in: T. Platt (Ed.), Physiological Bases of Phytoplankton Ecology," *Can. Bull. Fish. Aquat. Sci.*, vol. 210, pp. 182–210, 1981.
[41] Eilers PHC, Peeters JCH. A model for the relationship between light intensity and the rate of photosynthesis in phytoplankton. Ecol Model 1988;42(3–4):199–215. https://doi.org/10.1016/0304-3800(88)90057-9.
[42] Sager J, McFarlane C. *Plant Growth Chamber Handbook*, North Cent. NCERA-101 Committee on Controlled Environment Technology and Use 1997.
[43] Jacovides CP, Tymvios FS, Asimakopoulos DN, Theofilou KM, Pashiardes S. Global photosynthetically active radiation and its relationship with global solar radiation in the Eastern Mediterranean basin. Theor Appl Climatol 2003;74(3–4):227–33. https://doi.org/10.1007/s00704-002-0685-5.
[44] Dauta A, Devaux J, Piquemal F, Boumnich L. Growth rate of four freshwater algae in relation to light and temperature. Hydrobiologia 1990;207(1):221–6. https://doi.org/10.1007/BF00041459.
[45] Caballero PB. Analysis and characterization of the atmospheric surface layer. University of Barcelona; 2003.
[46] Tchobanoglous G, Burton FL, Stensel HD. Wastewater Engineering: Treatment and Reuse. New York: Tchobanogl; 2003.
[47] Couto E, Calijuri ML, Assemany P, Cecon PR. Evaluation of high rate ponds operational and design strategies for algal biomass production and domestic wastewater treatment. Sci Total Environ 2021;791:148362. https://doi.org/10.1016/j.scitotenv.2021.148362.
[48] Tsagarakis KP, Mara DD, Horan NJ, Angelakis AN. Small municipal wastewater treatment plants in Greece. Water Sci Technol 2000;41(1):41–8. https://doi.org/10.2166/wst.2000.0007.
[49] Vera I, Sáez K, Vidal G. Performance of 14 full-scale sewage treatment plants: Comparison between four aerobic technologies regarding effluent quality, sludge production and energy consumption. Environ. Technol. (United Kingdom) 2013;34(15):2267–75. https://doi.org/10.1080/09593330.2013.765921.
[50] Tsihrintzis VA, Gikas GD. Constructed wetlands for wastewater and activated sludge treatment in north Greece: A review. Water Sci Technol 2010;61(10):2653–72. https://doi.org/10.2166/wst.2010.188.
[51] E. Ortega, Y. Ferrer, J. . Sala, C. Aragón, and Á. Real, *Manual para la implantación de sistemas de depuración en pequeñas poblaciones*. 2010.
[52] Ferrer J. "Sistemas de control y optimización del consumo energético en EDAR. XXX Curso Tratamiento de Aguas Residuales y Explotación de EstacionesDepuradoras. Centro de Estudios y Experimentación de Obras Públicas (CEDEX). Madrid": Gobierno de España; 2012.
[53] Hernández-Sancho F, Lamizana-Diallo B, Mateo-Sagasta M, Qadir M. Economic Valuation of Wastewater: The Cost of Action and the Cost of No Action, 2015.
[54] Pajares EM, Valero LG, Sánchez IMR. Cost of urban wastewater treatment and ecotaxes: Evidence from municipalities in southern Europe. Water (Switzerland) 2019;11(3):1–13. https://doi.org/10.3390/w11030423.